First-Principles Modelling of Electrospraying, and the Effects of Dissipation in Electrospray Thrusters

IEPC-2017-149

Presented at the 35th International Electric Propulsion Conference
Georgia Institute of Technology • Atlanta, Georgia • USA
October 8 – 12, 2017

M. Gamero-Castaño[1]
University of California, Irvine, California 92717, USA

Abstract: This paper describes on-going work on the development of a first-principles model of electrospraying operating in the cone-jet mode. In particular, the model includes: a) the equations of the leaky dielectric model (i.e. conservation of mass, momentum and surface charge; the Laplace equation for the electrostatic potential; and the Young-Laplace equation for the position of the free surface); b) a novel energy conservation equation to reproduce the non-homogeneous temperature field caused by energy dissipation (propellant properties retains their dependence on temperature); and c) realistic boundary conditions. The model is solved numerically, and model outputs such as the beam current and the position of the surface are compared to an existing numerical solution.

Nomenclature

c	=	fluid specific heat
D	=	jet diameter
E	=	electric field
e	=	elementary unit charge
h	=	Planck's constant
j''	=	ion evaporation flux
k_B	=	Boltzmann's constant
K	=	fluid electrical conductivity
m	=	droplet mass
Q	=	volumetric flow rate
Q_{FM}	=	dimensionless flow rate
q	=	droplet charge
Re_K	=	fluid-properties Reynolds number
$R(x)$	=	position of the surface of the cone-jet
r	=	radial independent variable
T	=	temperature
v	=	velocity
v_S	=	surface velocity
x	=	axial independent variable
ε_0	=	permittivity of the vacuum
ε	=	fluid dielectric constant
ρ	=	fluid density

[1] Associate Professor, Department of Mechanical and Aerospace Engineering, mgameroc@uci.edu.

γ = fluid surface tension
Δ = voltage deficit
ΔT = temperature increase
ΔG_S^0 = ion solvation energy
μ = fluid viscosity
ϕ = electric potential
σ = surface charge density

I. Introduction

ELECTROSPRAY propulsion (ESP) is an electric propulsion technology based on the electrostatic acceleration of charged droplets and ions emitted by an electrospray. Due to its central role, a fundamental understanding of electrospraying is key for developing ESP. Electrospraying is known for generating sprays of droplets with average diameters ranging from tens of microns to a few nanometers. The nanometric regime is the one of interest to ESP, because the charge-to-mass ratio *q/m* of the atomized droplets and the specific impulse, $Isp \propto (q/m)^{1/2}$, increase at decreasing droplet diameter, and this technology must operate at maximum *Isp* to be of interest. For a given propellant the maximum charge-to-mass ratio and minimum jet diameter scale as:

$$< q/m >_{\max} \cong a(\varepsilon)\left(\varepsilon_0/\rho\right)^{1/2} \text{ K} \tag{1}$$

$$D_{\min} \cong \left(\varepsilon^{1/2}\varepsilon_0^2\gamma/\rho\right)^{1/3}/K^{2/3} \tag{2}$$

$a(\varepsilon)$ is a function of the dielectric constant of order 1. The electrical conductivity is the only propellant property that can be varied by many orders of magnitude, and therefore high *Isp* operation implies the use of propellants of high conductivity (typically higher than 1 S/m). The nanometric, or high conductivity regime is heavily influenced by two phenomena: intense energy dissipation that causes strong temperature gradients; and the onset of ion field evaporation. Dissipation has never been modeled or accounted for, and as a result ESP is currently developed on the bases of empirical information and the extrapolation of scaling laws.

The importance of energy dissipation has been determined recently.[1] Experiments have shown that the stopping voltage of electrospray droplets is smaller than the voltage applied to the emitter electrode. The difference Δ can be interpreted as a voltage deficit or irreversible loss of energy (per unit charge) needed to form the drops. The voltage deficit results from the dissipation of mechanical and electrical energy, together with the generation of surface energy. Experimentally Δ is known to have the following dependency:[1]

$$\frac{\Delta}{\phi_0} = \alpha(\varepsilon) + \beta(\varepsilon)\frac{1}{Re_K} \tag{3}$$

where $Re_K = \rho^{1/3}\varepsilon_0^{1/3}\gamma^{2/3}/(\mu K^{1/3})$ and $\phi_0 = \gamma^{2/3}/(K^{1/3}\varepsilon_0^{1/6}\rho^{1/6})$. Δ increases with decreasing electrical conductivity, and is independent of the flow rate. The associated dissipation is estimated to increase the temperature of the propellant in the amount:

$$\Delta T \cong \frac{a(\varepsilon)\beta(\varepsilon)}{c}\left(\frac{\mu^2\gamma K}{\varepsilon_0 Q\rho^3}\right)^{1/2}, \qquad \Delta T \cong \frac{a(\varepsilon)\beta(\varepsilon)}{c}\frac{\mu}{\varepsilon_0\rho}K \quad \text{at } Q_{\min} \tag{5}$$

ΔT is proportional to the electrical conductivity, and is substantial in cone-jets with the high K values required by the nanometric regime: e.g. we estimate values exceeding 100 ºC for formamide solutions with conductivities exceeding 1 S/m, and for ionic liquids like EMI-Im. Key propellant properties such as K and μ, as well as the rate of ion evaporation, depend strongly on temperature. Clearly the large temperature gradients occurring in the nanometric regime must be accounted for by any realistic model for ESP.

The ions that accumulate on the surface of the cone-jet evaporate when the repelling electrostatic force overcomes the attractive forces exerted by surrounding molecules. Ion field evaporation is a kinetic process with an energy barrier lowered by the electric field E in the amount $G_E = (e^3 E / 4\pi\varepsilon_0)^{1/2}$ (e is the elementary charge). The evaporation flux ($\mathrm{Cm^{-2}s^{-1}}$)is given by:[2]

$$j'' \cong \frac{k_B T}{h} \sigma \exp\left[-\frac{\Delta G_S^0 - G_E}{k_B T} \right] \tag{6}$$

Due to the exponential dependence on E, evaporation only becomes substantial when the electric field exceeds a critical value, typically of the order of 1 V/nm. Using scaling laws (1) and (2) to estimate the maximum electric field in the cone-jet:[2]

$$E_{\max} \cong \frac{\gamma^{1/2} K^{1/6}}{\varepsilon_0^{2/3} Q^{1/6}}, \qquad E_{\max} \cong \frac{\rho^{1/6} \gamma^{1/3} K^{1/3}}{\varepsilon_0^{5/6}} \text{ at } Q_{\min} \tag{7}$$

it can be determined that $E_{max} \cong 1$ V/nm at conductivities near 1 S/m, triggering ion evaporation. In fact, it is well known that the beams of all good propellants (i.e. those with the highest *Isp*) emit a combination of charged droplets and evaporated ions.[3,4] It would be highly desirable to increase K further to increase *q/m* and the *Isp*, but doing so augments E, the emission of ions, and propulsive inefficiencies associated with the very dissimilar exhaust velocities of ions and droplets. Even worse, significant ion evaporation makes the electrospray unstable, an observation for which a theoretical explanation does not exist. Very little experimental information is available on the effects of ion field evaporation on ESP, and this key phenomenon, including the obvious coupling with dissipation through the temperature dependence of the evaporation rate, has not been modeled in any detail.

There are several theoretical models of electrospraying in the cone-jet mode, but none addresses the particular physics of the nanometric regime. Most models divide the cone-jet into three sequential regions: the Taylor cone,[5] a static region in which ohmic conduction is the dominant current mechanism; a transition region between the cone and the jet where charge is injected on the surface, and convected surface charge progressively replaces bulk conduction; and a jet accelerated by electrical forces, where surface current is the dominant transport mechanism. The analysis of the transition region is the central problem in these theories because the current and the diameter of jet are fixed in this area, controlled by local parameters largely insensitive to the variations of the geometry and electrostatics in the far field. Fernández de la Mora & Loscertales produced the first modern seminal work on the modeling of cone-jets, and were able to explain the *I(Q)* law by considering a transition region dominated by electrical relaxation phenomena.[6] In contrast, Gañán-Calvo inferred that the surface charge is in equilibrium throughout the cone-jet, and obtained alternative scaling laws for the current and jet diameter based on this idea.[7] Gañán-Calvo has also analyzed the jet by coupling its dynamics with the electric field induced by the Taylor cone,[8] an idea that makes it possible to formulate a local model of the transition region with asymptotic, far-field boundary conditions. Higuera has integrated the complete set of partial differential equations for the transition region, and has also studied several asymptotic limits.[9] The work of Collins et al., who seek to numerically solve the complete set of equations in the cone-jet and surrounding electrostatic domain, is a departure from the models centered in the transition region.[10] The main problem of these models is that none includes ion field evaporation, nor the strong temperature gradients taking place in the nanometric regime, and therefore they are of limited applicability to electrospray propulsion. We are currently developing a model of cone-jets relevant to ESP, and this article describes our initial work in this problem.

II. Cone-Jet Model

A. Model Equations

Figure 1 shows a simplified domain helpful for the description of the cone-jet model. The cone-jet is enclosed by surfaces $\Gamma_1^i \cup \Gamma_2^i$, where the index *i* stands for inner domain; the fluid is surrounded by vacuum, which forms the outer domain enclosed by $\Gamma_1^o \cup \Gamma_2^o$. Γ_1 is the surface of the cone-jet, and its position is described by the function $R(x)$. The basic unknowns of the model are the fluid's velocity $\mathbf{v}(\mathbf{x})$ and temperature $T(\mathbf{x})$ fields, the charge density $\sigma(x)$ in the surface of the cone-jet, the position of the surface $R(x)$, and the electric potential fields in the fluid $\phi^i(\mathbf{x})$ and surrounding $\phi^o(\mathbf{x})$ domains. The basic differential equations relating these unknowns are:

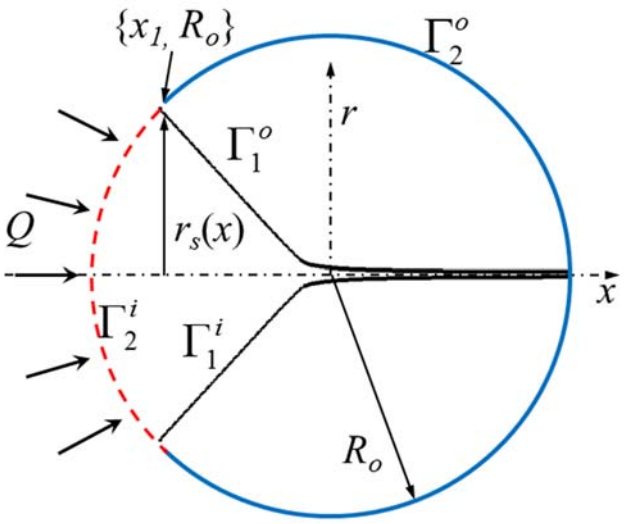

Figure 1. Model Domain.

$$\left.\begin{aligned} \nabla\cdot\mathbf{v}=0 \quad (8.1), \qquad \rho\,\mathbf{v}\cdot\nabla\mathbf{v} &= -\nabla p+\mu\nabla^2\mathbf{v} \quad (8.2)\\ \rho c\,\mathbf{v}\cdot\nabla T=\nabla\cdot(k\,\nabla T)+\boldsymbol{\tau}_\mu\!:\!\nabla\mathbf{v}+\mathbf{E}\cdot\mathbf{J} \quad (8.3), \qquad \nabla^2\phi^i &= 0 \quad (8.4)\end{aligned}\right\} \text{ for } r<R(x) \tag{8}$$

$$\frac{\mathrm{d}(R\upsilon_S\,\sigma)}{\mathrm{d}x}=R\left(K\,E_n^i-\frac{k_BT}{h}\sigma\exp\left[-\frac{\Delta G_S^0-G_E(E_n^o)}{k_BT}\right]\right)\sqrt{1+R'^2} \qquad \text{at } r=R(x) \tag{9}$$

$$\nabla^2\phi^o=0 \qquad \text{for } r>R(x) \tag{10}$$

Constraints must be imposed at the surface of the fluid: a) the surface must be in mechanical equilibrium (the balance of stresses along the normal yields a Laplace-Young equation for the position of the surface including the electrostatic stress (11.1), and a tangential term accelerating the fluid (11.2)); c) the jump conditions for the normal (11.3) and tangential (11.4) components of the electric field across the interface of a charged dielectric; and d) the surface kinematic condition (11.5):

$$\left.\begin{aligned} \gamma\frac{R'^2-RR''+1}{R(1+R'^2)^{3/2}} &= p-\mathbf{n}\cdot\boldsymbol{\tau}_\mu\cdot\mathbf{n}+\frac{\varepsilon_0}{2}\left(E_n^{o2}-\varepsilon E_n^{i2}\right)+\frac{\varepsilon_0}{2}(\varepsilon-1)E_t^2 \quad (11.1)\\ \mathbf{t}\cdot\boldsymbol{\tau}_\mu\cdot\mathbf{n} &= \sigma E \quad (11.2)\\ \sigma=\varepsilon_0(E_n^o-\varepsilon E_n^i) \quad (11.3), \quad E_t^i=E_t^o \quad (11.4), \quad \mathbf{v}\cdot\mathbf{n}&=0 \quad (11.5)\end{aligned}\right\} \text{ at } r=R(x) \tag{11}$$

Additional boundary conditions are an upstream prescribed velocity profile with flow rate Q (we use a spherical sink flow), and prescribed potentials at the outer surfaces; we use the potential derived by Taylor in his classical work:[5]

$$\mathbf{v}(\Gamma_2^i)=\mathbf{g} \quad (12), \qquad \phi^i=f_1(x) \text{ at } \Gamma_2^i \quad (13), \qquad \phi^o=f_2(x) \text{ at } \Gamma_2^o \quad (14)$$

The model stated above is well-posed, but solving this system is not trivial. The main difficulties arise from the non-linear nature of most equations, the strong coupling between several of them, and the presence of a free-surface: the position of the cone-jet's surface is not known a priori, but is part of the solution. In order to derive an iterative algorithm to find the solution, we divide the equations into three groups referred to as the fluid problem (equations (8.1), (8.2), (8.3), (11.2), (11.5) and (12)), the electrical problem (equations (8.4), (9), (10), (11.3), (11.4), (13), and (14)), and the Young-Laplace equation, (11.1) for the surface. For a given position of the surface, the fluid problem

and the electrical problem are readily solved in iterative fashion since their only coupling is through both the tangential component of the stress present as a boundary condition at Γ_1^o in the fluid problem, and the surface velocity in the equation of conservation of charge in the electrical problem. Once this fluid-electrical solution is found for a given surface profile, the Young-Laplace equation can in principle be used to update the position of the surface, which in turn is used to compute an updated fluid-electrical solution. This iterative process is continued until the residues of the different equations are smaller than desired values.

The continuity and momentum equations of the fluid problem are solved using the stream function/vorticity formulation. This approach is standard in two-dimensional and axisymmetric flows like this one, because it allows reducing the system of three equations for three dependent variables (two velocity components and the pressure), to a system of two elliptic PDEs for the stream function Ψ and the vorticity Ω. Once the stream function and vorticity fields are determined, the pressure is readily obtained by integrating the momentum equation along the surface. We discretize the PDEs using finite differences in an orthogonal grid. The results presented in this article do not include the solution of the energy equation (8.3), which will be done at a later stage of the research.

To update the surface using the Young-Laplace equation we use a least-square integral method that minimizes the global error of (11.1), i.e. the updated surface results from the minimization of

$$\int_{\Gamma_1}\left[\gamma\frac{R'^2 - R\,R'' + 1}{R\,(1+R'^2)^{3/2}} - \left(P - \mathbf{n}\cdot\boldsymbol{\tau}_\mu\cdot\mathbf{n} + \frac{\varepsilon_0}{2}\left(E_n^{o\,2} - \varepsilon E_n^{i\,2}\right) + \frac{\varepsilon_0}{2}(\varepsilon-1)E_t^2\right)\right]^2 dx \tag{15}$$

To minimize equation (15) for given values of the pressure and the viscous and electrical stresses, $R(x)$ is discretized into N nodes R_i, i = 1, 2, …, N, and the derivative of the integral with respect to each R_i is made equal to zero. This yields a system of N algebraic nonlinear equations, which can be solved iteratively using the Newton method. We do not use the converged solution of the Newton method as the updated position of the surface, but the value provided by the first iteration.

We solve the equations in dimensionless form, using the following length, velocity, pressure and current scales:

$$r_c = \left(\frac{\rho\varepsilon\varepsilon_0 Q^3}{\gamma K}\right)^{1/6} \tag{16}$$

$$v_c = \frac{Q}{\pi r_c{}^2} \tag{17}$$

$$P_c = \frac{\gamma}{r_c} \tag{18}$$

$$I_c = (\gamma K Q)^{1/2} \tag{19}$$

The dimensionless equations include the dielectric constant ε and two additional dimensionless numbers, which can be expressed in multiple ways. Our choices are the dimensionless flow rate Q_{FM}, $Q_{FM} = \rho K Q/(\gamma\varepsilon\varepsilon_0)$, and Re_K.

B. Algorithm for Solving the System of Equations

The system of partial differential and algebraic equations is highly nonlinear. Once discretized, we use the following iterative algorithm to obtain numerical solutions for the associated system of algebraic equations:

1) Initial profiles for the surface and surface velocity are defined.
2) The fluid and electrical problems are solved for the given surface profile
   2.1. Equations (8.4), (9), and (10) are solved using the given surface and surface velocity profiles. The Boundary Element Method (BEM) with linear

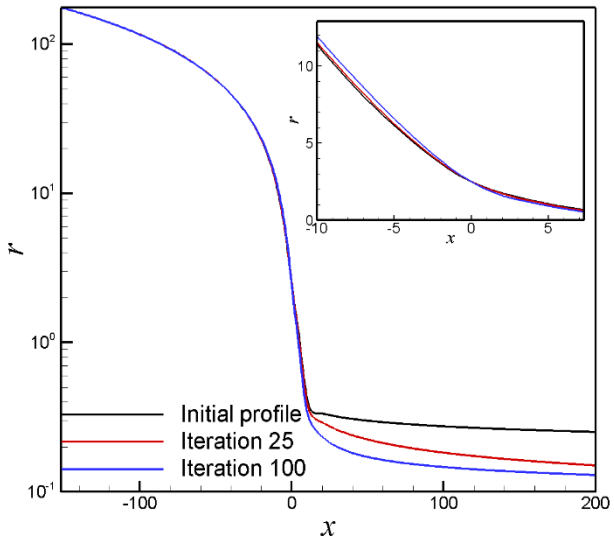

Figure 2. Initial cone-jet profile and profiles at iteration numbers 25 and 100.

elements is used to solve the Laplace equations for the electrical potentials, while the equation of conservation of charge is discretized using centered finite differences. This produces a linear system of equations for the potentials/normal electric fields at all boundary nodes, and the surface charge at nodes of surface profile.

2.2. The solution obtained in Step 2.1 is used to compute the boundary condition for the vorticity at the surface. With this information, the vorticity and stream function fields are computed.

2.3. The updated surface velocity is used to execute steps 2.1 and 2.2, which are repeated until the errors of the fluid and electrical variables are below a desired minimum, for the given surface profile.

3) The solution obtained in Step 2 is used to compute the pressure, electrical and viscous stress terms in the Young-Laplace equation, and the residue of this equation for the given profile. If the residue is smaller than a desired value the existing surface profile, and velocity, potential and surface charge fields are the desired numerical solution. Otherwise Step 4 is executed.

4) An updated solution for the surface profile is obtained using the least-squares method and the solution obtained in Step 2. Step 2 is then executed with the updated surface profile.

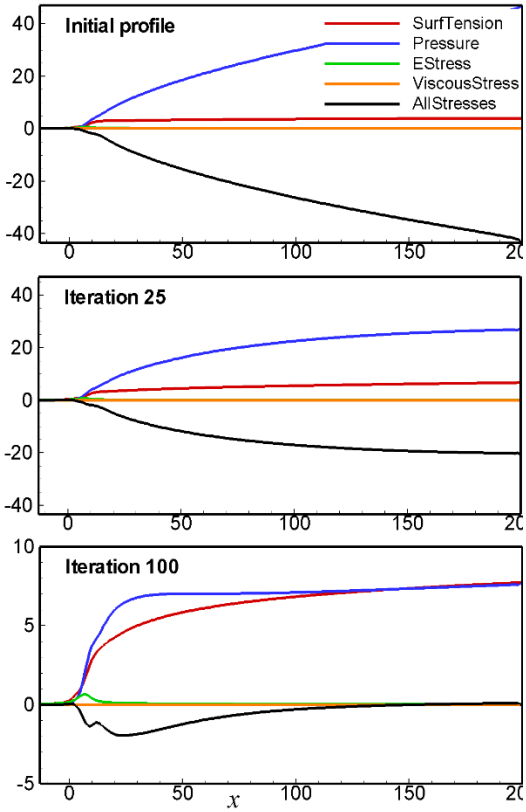

Figure 3. Normal stresses on the surface, for the initial profile and at iterations 25 and 100.

Figures 2-4 illustrate the algorithm, for a run simulating a cone-jet with electrospraying parameters $\mathcal{E}$ = 5, Re_K = 1, and Q_{FM} = 0.054. Figure 2 shows the initial surface profile, together with the profiles at iteration numbers 25 and 100. The ordinate is in logarithmic coordinates to better display the changes of the profile in the jet region; a detail of the region near the tip of the cone is also shown. The initial profile is constructed so that the profile matches a Taylor cone (half-cone angle of 49.3 deg) upstream, and an expected $R \sim x^{-1/8}$ law downstream, far from the tip of the cone. These two limits are joined smoothly around the base of the cone. As the iterations proceed the jet progressively becomes narrower than the initial guess, the base of the cone develops a sharper outline, and the upstream profile becomes very slightly convex.

Figure 3 shows the surface tension, the pressure, and the normal components of the electrical and viscous stresses along the surface, together with their balance (i.e. the different terms in the Young-Laplace equation), at these three iteration stages. The balance, which is indicative of the error of each solution, decreases as the algorithm advances.

Finally, Figure 4 shows the residue of the Young-Laplace equation as a function of the iteration number. The residue becomes smaller as the run proceeds, i.e. the numerical solution progressively gets closer to the physical solution. The rate at which the residue decreases changes substantially at iterations 100, 140 and 152. This is due to manual changes in two parameters of the least-square optimization routine, which control the speed vs. stability of the convergence.

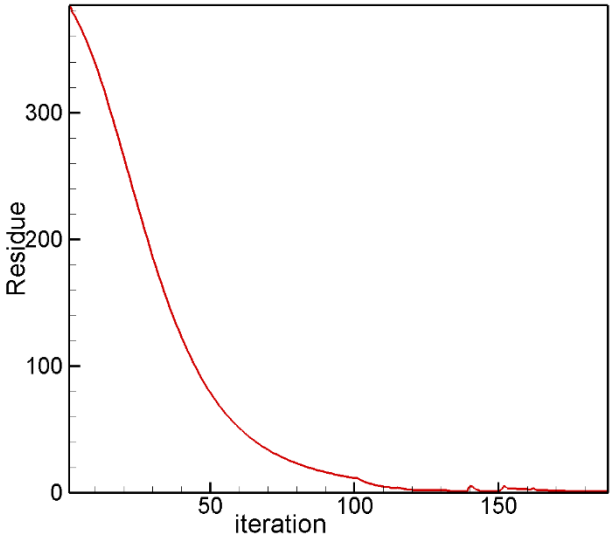

Figure 4. Evolution of the residue of the Young-Laplace equation.

III. Numerical Solution

The solution for the electrospraying state $\mathcal{E} = 5$, $Re_K = 1$, and $Q_{FM} = 0.054$ is illustrated in Figures 5 to 9. This final solution corresponds to iteration 188 in Figure 4. We choose this state because the same conditions have been investigated by Higuera,[9] making the comparison of our numerical solution with published data possible. Figure 5 shows the profile of the cone-jet, and an insert with the region near the origin together with points extracted from Higuera's solution. The axial coordinates of Higuera's poinst have been shifted forward $1.4r_C$ units to better match our solution: when using Taylor's potential as the far-field boundary condition for the electrical problem, the uncertainty in the position of the origin of the axial coordinate is of the order of r_C. Although both Higuera and the present work use this boundary condition, we suspect that Higuera imposes the boundary much closer to the tip of the cone than us: we place it at a distance of $200r_C$ from the tip, while based on Higuera's figures, he seems to impose it at approximately $10r_C$. If true, Higuera's harder constraint should make his solution less representative of the physical state than ours. Although the two profiles have been computed using significantly different methods, they match well, supporting the validity of both solutions.

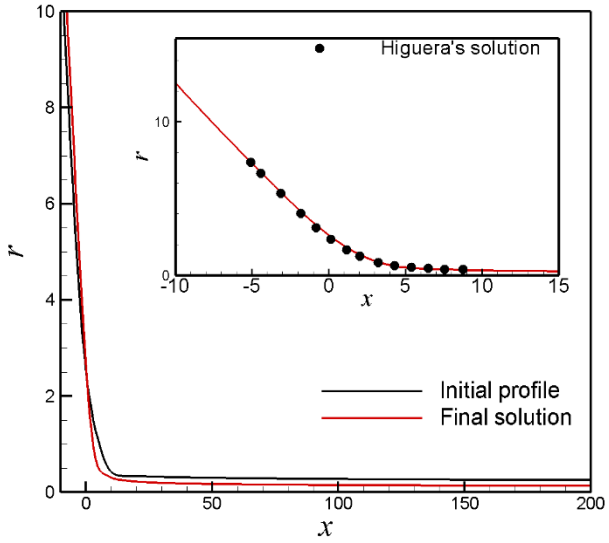

Figure 5. Initial and final profile for $\mathcal{E} = 5$, $Re_K = 1$, and $Q_{FM} = 0.054$. The profile matches well Higuera's solution for the same electrospraying parameters.

Figure 6 shows the evolution of the conduction and surface currents along the axial coordinate, and the total current. The conduction and surface currents across a plane of constant x are defined by:

$$I_C(x) = \int_0^{R(x)} 2\pi\, rKE_x^i(x,r)dr \tag{20}$$

$$I_S(x) = 2\pi\, R(x)v_S(x)\sigma(x) \tag{21}$$

The total current crossing a plane of constant x is the sum of the two, and should be independent of x due to conservation of charge. The conduction current dominates upstream, and progressively diminishes in the cone-to-jet transition as charge is transferred towards the surface. The total current increases with x, has an average value of 2.45 and a standard deviation of 0.11. The total current is not constant due to the relatively coarse grid used in these calculations, but this error can be arbitrarily reduced by increasing the resolution of the grid. The current reported by Higuera for this case is 2.12.

Figure 7 shows contour maps of the stream function and the vorticity. The flow is accelerated by the tangential component of the electric stress on the surface, creating in the cone region a relatively thin layer of high velocity parallel to the surface and a larger recirculation region surrounding the axes. The upstream boundary condition for the velocity (sink flow) is somewhat artificial, and results on unphysically low surface velocities at the upstream boundary for the domain of the flow problem. This produces an abrupt increase of the surface current

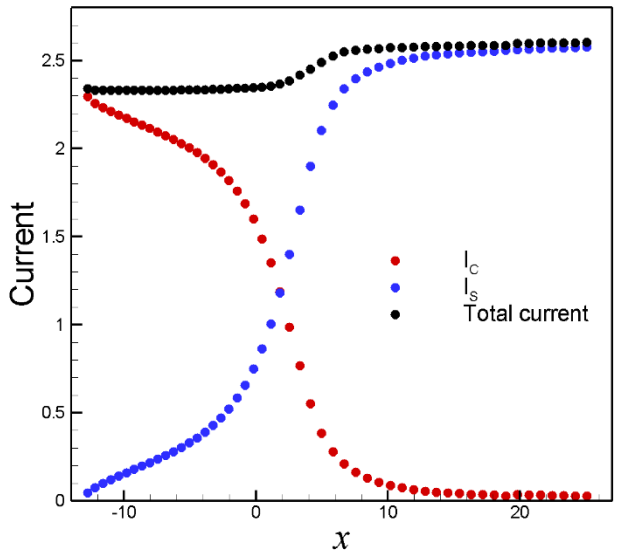

Figure 6. Initial and final profile for $\mathcal{E} = 5$, $Re_K = 1$, $Q_{FM} = 0.054$. The profile matches well Higuera's solution for the same electrospraying parameters.

at the intersection of this boundary with the surface (i.e. the values of the surface current at the smallest values of x in Figure 6 should be slightly larger), but should not alter substantially the overall solution nor the value of the average current. The tangential electric stress on the surface is the source of vorticity in this system, and is most intense at the base of the jet where the transfer of charge to the surface peaks.

Figure 8 shows the capillary stress, the pressure, and the normal components of the viscous and electrical stresses. The normal component of the viscous stress is negligible everywhere. The electrical stress fully balances the capillary stress upstream; all three pressure, capillary stress and electrical stress are significant in the balance of normal forces at the tip of the cone; and the electrical stress is marginal along the jet, where the pressure and capillary stress almost fully balance each other.

Figure 9 shows the electric variables on the surface of the cone-jet: the potential, the tangential and normal (both inside the fluid and the surrounding vacuum) components of the electric field, and the surface charge.

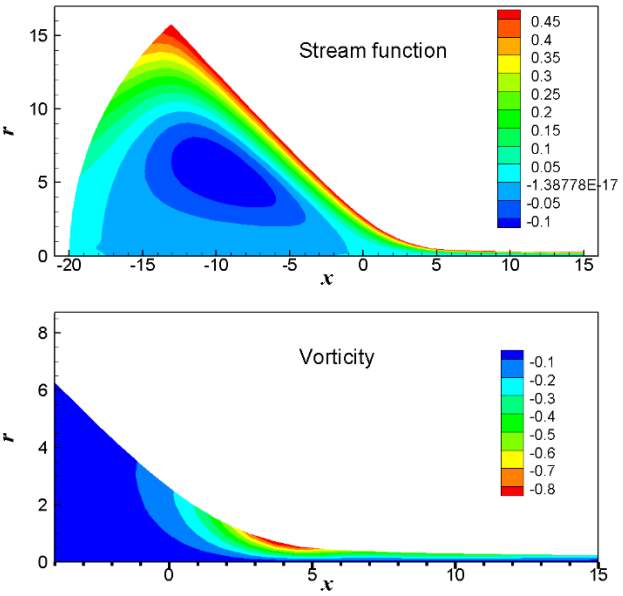

Figure 7. Contour maps of the stream function and vorticity for $\mathcal{E}$ = 5, Re_K = 1, Q_{FM} = 0.054. .

The surface of the cone is equipotential, and only around x = 0 the potential starts decreasing and the tangential component of the electric field becomes significant. The tangential and the normal component of the outer field peak at x = 5.6, while the normal component of the inner field peaks further downstream at x = 10.5. Although the normal component of the inner field has a negligible contribution to the electric stress anywhere, it is important in the equations for the surface charge, (11.3), at its peak: $E_n^o = 1.48$ and $\varepsilon E_n^i = 0.91$ at x = 10.5.

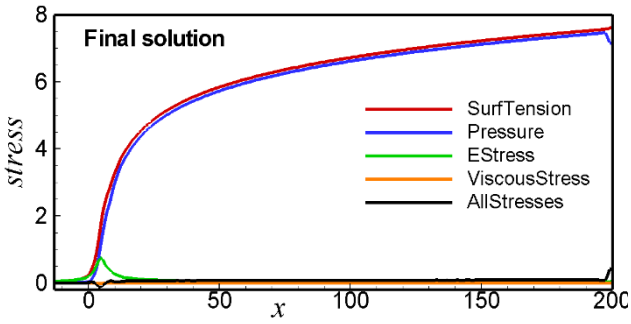

Figure 8. Normal stresses on the surface for $\mathcal{E}$ = 5, Re_K = 1, and Q_{FM} = 0.054.

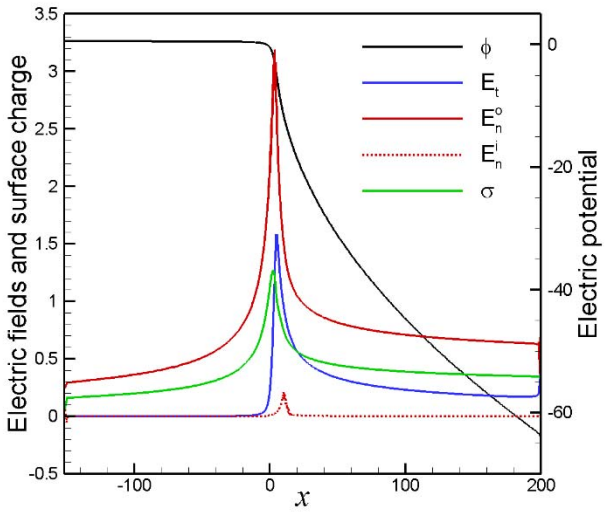

Figure 9. Electric potential, tangential and normal components of the electric field, and surface charge along the surface for $\mathcal{E}$ = 5, Re_K = 1, Q_{FM} = 0.054.

IV. Conclusion

We have described an electric-fluid dynamic model of cone-jets, based on the leaky-dielectric model.[11] The model includes the effect of energy dissipation and the resulting non-homogeneity of the temperature field and fluid properties, but this aspect has not been included yet in the discretized equations. Besides the inclusion of dissipation, the main novelties of our model are the use of a least-square integral method for solving the Young-Laplace equation (and hence to impose the required balance of normal stresses on the surface), and the placement of the far-field boundary conditions at a distance from the cone-to-jet transition orders of magnitude larger than the characteristic length of the transition region. The initial algorithm used to solve the model equations converges to the physical solution. Future work will address the development of a more robust algorithm, the inclusion of dissipation effects, and the analysis of the results especially as related to electrospray propulsion.

Acknowledgments

This research was supported by NASA's Space Technology Research Early Stage Innovations program, grant NNX17AD01G, and by NSF's Fluid Dynamics program, grant CBET-1604163. We are thankful for the support of the NASA Research Collaborator John Yim, and the NSF program manager Dr. Ronald Joslin.

References

1 Gamero-Castaño, M., "Energy dissipation in electrosprays and the geometric scaling of the transition region of cone-jets", Journal of Fluid Mechanics, Vol. 662, 2010, pp. 493, 513.

2 Gamero-Castaño, M., and Fernández de la Mora, J., "Direct measurement of ion evaporation kinetics from electrified liquid surfaces", Journal of Chemical Physics, Vol. 113, 2000, pp. 815, 832.

3 Gamero-Castaño, M., "Electric-field-induced ion evaporation from dielectric liquid", Physical Review Letters, Vol. 89, 2002, 147602.

4 Gamero-Castaño, M., "Characterization of the electrosprays of 1-Ethyl-3-Methylimidazolium Bis(Trifluoromethylsulfonyl) Imide in vacuum", Physics of Fluids, Vol. 20, 2008, 032103.

5 Taylor, G. I., "Disintegration of water drops in an electric field", Proceedings of the Royal Society of London A, Vol 280, 1964, pp. 383,397.

6 Fernández de la Mora, J., and Loscertales, I.G., "The current transmitted through an electrified conical meniscus", Journal of Fluid Mechanics, Vol. 260, 1994, pp. 155,184.

7 Gañán-Calvo, A. M., "On the general scaling theory for electrospraying", Journal of Fluid Mechanics, Vol. 507, 2004, pp. 203, 212.

8 Gañán-Calvo, A. M., "Cone-jet analytical extension of Taylor's electrostatic solution and the asymptotic universal scaling laws in electrospraying", Physical Review Letters, Vol. 79, 1997, pp. 217, 220.

9 Higuera, F. J., "Flow rate and electric current emitted by a Taylor cone", Journal of Fluid Mechanics, Vol. 484, 2003, pp. 303, 327.

10 Collins, R. T., Harris, M. T., and Basaran, O. A., "Breakup of electrified jets", Journal of Fluid Mechanics, Vol. 588, 2007, pp. 75, 129.

[11] Saville, D. A., "Electrohydrodynamics: The Taylor-Melcher Leaky Dielectric Model", Annual Review Fluid Mechanics, Vol. 29, 1997, pp. 27, 64.